Published in final edited form as:
Bioconjug Chem. 2012 March 21; 23(3): 610–617. doi:10.1021/bc200654v.

Biomineralization and Size Control of Stable Calcium Phosphate Core Protein Shell Nanoparticles: Potential for Vaccine Applications

David Chiu[†,a], **Weibin Zhou**[†,a], **Sathana Kitayaporn**[†], **Daniel T. Schwartz**[†], **Kaja Murali-Krishna**[‡,b], **Terrance J. Kavanagh**[§], and **François Baneyx**[†,*]

[†]Department of Chemical Engineering, University of Washington, Seattle, WA 98195

[‡]Department of Immunology, University of Washington, Seattle, WA 98195

[§]Department of Environmental and Occupational Health Sciences, University of Washington, Seattle, WA 98195

Abstract

Calcium phosphate (CaP) polymorphs are nontoxic, biocompatible and hold promise in applications ranging from hard tissue regeneration to drug delivery and vaccine design. Yet, simple and robust routes for the synthesis of protein-coated CaP nanoparticles in the sub-100 nm size range remain elusive. Here, we used cell surface display to identify disulfide-constrained CaP binding peptides that, when inserted within the active site loop of *E. coli* Thioredoxin 1 (TrxA), readily and reproducibly drive the production of nanoparticles that are 50–70 nm in hydrodynamic diameter and consist of an approximately 25 nm amorphous calcium phosphate (ACP) core stabilized by the protein shell. Like bone and enamel proteins implicated in biological apatite formation, peptides supporting nanoparticle production were acidic. They also required presentation in a loop for high affinity ACP binding since elimination of the disulfide bridge caused a nearly 3-fold increase in hydrodynamic diameters. When compared to a commercial aluminum phosphate adjuvant, the small core-shell assemblies led to a 3-fold increase in mice anti-TrxA titers three weeks post-injection, suggesting that they might be useful vehicles for adjuvanted antigen delivery to dendritic cells.

INTRODUCTION

Because they are highly biocompatible and nontoxic, calcium phosphate (CaP) nanoparticles have been explored in applications ranging from hard tissue regeneration to the delivery of small molecules, oligonucleotides, and proteins.[1, 2] CaP also holds promise as a vaccine adjuvant[3–5] where nanoscale formulations have been shown to be more effective than micrometer-sized particles at targeting lymph node dendritic cells (DCs) for enhancing immunity.[6, 7] Unfortunately, unstabilized CaP colloids have a strong tendency to aggregate, and their controlled synthesis is challenging because even small variations in pH, temperature, calcium to phosphate ratio, or precipitation technique can significantly affect particle stoichiometry, crystallinity, morphology, and size.[8–10] A wide variety of CaP synthesis schemes have been developed, ranging from microemulsion technologies,[11–13] to the use of citrate,[14] surfactants,[15] porphyrin,[16] and oligonucleotides,[17] as capping agents. However, reproducible production of stable CaP colloids in the sub-100 nm range remains

[*]Corresponding Author: Telephone: +1 206 6857659; Fax: +1 206 6853451; baneyx@uw.edu.
[a]Contributed equally to this work
[b]Current address: Department of Pediatrics, Emory University School of Medicine, Atlanta, GA 30322

difficult, and their controlled conjugation with peptides or proteins by any mechanism other than adsorption requires multiple chemical derivatization and purification steps.

In vertebrate bones, CaP is present in the form of hydroxyapatite (HA; $Ca_{10}(PO_4)_6(OH)_2$) nanocrystals that are 30–50 nm long, 20–25 nm wide and 1.5 to 4 nm thick.[18] These nanoplates are embedded in a composite of collagen fibrils and non-collagenous proteins that exhibit Ca^{2+} and hydroxyapatite binding properties by virtue of being phosphorylated and rich in negatively charged (acidic) residues.[19] Several non-collagenous phosphoproteins have been shown to promote HA nucleation and to control the kinetics of crystal growth,[19, 20] suggesting that they may be good candidates for the biomimetic mineralization of CaP nanoparticles. However, the same proteins can also inhibit mineralization, and the mechanisms that are at play for either process remain unclear and controversial.[19, 20]

Solid binding peptides (SBPs) isolated by phage or cell surface display[21] present an alternative to naturally occurring proteins for the biomineralization of technologically valuable materials,[22] In this molecular biomimetic approach to material synthesis, SBPs are used either in isolation or as part of a larger protein or organism to nucleate, organize and assemble inorganic structures with nanoscale control of composition and architecture.[23, 24] The approach is powerful. For example, we have shown that “designer proteins” incorporating SBPs can be used to nucleate and cap Cu_2O nanoparticles under thermodynamically unfavorable conditions,[25] organize these nanoparticles onto DNA guides,[25] control the size and shape of silver crystals,[26] and mineralize multicolored ZnS quantum dots whose protein shell is active for antibody binding.[27, 28]

Here, we describe disulfide-constrained CaP binding peptides that, when inserted within the active site loop of *E. coli* Thioredoxin 1 (TrxA), reproducibly mineralize nanoparticles that are 50–70 nm in hydrodynamic diameter and consist of an ≈ 25 nm amorphous calcium phosphate (ACP) core stabilized by a protein shell. We further show that disruption of the disulfide bond causes an increase of about 3-fold in the diameter of mineralized particles, indicating that the conformation of an SBP can have a profound influence on the mineralization process. Finally, we provide preliminary evidence that the small CaP core-protein shell nanoparticles might be effective vehicles for adjuvanted antigen delivery to DCs.

EXPERIMENTAL PROCEDURES

Electrodeposition of Calcium Phosphate on Titanium

CaP chips were synthesized using a modification of published protocols.[29, 30] Briefly, calcium phosphate was electrodeposited with a constant current of −2.5 mA/cm^2 for 20 min at 60°C on a 0.127 mm thick titanium foil (>99.9%; Sigma-Aldrich) from an electrolyte consisting of 100 mM $Ca(NO_3)_2$ and 50 mM $NH_4H_2PO_4$. All experiments were conducted in a quiescent 150 mL cell using a platinum wire for a counter-electrode. Half of the samples were annealed by heating for 8h at 450°C in an oven while the rest were N_2-dried.

Selection of CaP Binding Peptides

The FliTrx cell surface display system (Invitrogen) was used to select disulfide-constrained CaP-binding dodecapeptides through 5 rounds of biopanning as previously described.[28, 31] Independent selections were conducted on ~1 cm^2 annealed and non-annealed substrates. Randomly selected colonies (78 for annealed samples and 66 for non-annealed samples) were sequenced using the Big Dye Terminator sequencing kit (Applied Biosystems) using either 5′-ATTCACCTGACTGACGAC-3′ as a forward primer, or 5′-CCCTGATATTCGTCAGCG-3′ as a reverse primer. Six clones lacking internal cysteine

residues and exhibiting a broad range of hydrophobicities and isoelectric points (Table 1) were selected for further studies.

Construction, Expression and Purification of CaP Binding Proteins

Derivatives of *E. coli* thioredoxin 1 (TrxA) displaying disulfide constrained CaP binding peptides in place of the Cys-Gly-Pro-Cys active site sequence of native TrxA were constructed as previously described.[28] Briefly, pFliTrx derivatives encoding the target dodecapeptides were digested with *Apa*LI and *Rsr*II and the purified 220 bp fragment was ligated with the backbone of pT-Trx[32] that had been digested with the same enzymes. The resulting plasmids were named pTrxA-PAx or pTrxA-PNx where PA and PN refer to sequences selected on annealed (PA) or non-annealed (PN) CaP chips, and×denotes the numerical identifier of the CaP binding peptide. The Cys^{32} residue of TrxA::PA44 and TrxA::PN21 was converted to a serine by site directed mutagenesis of the corresponding plasmids using the QuikChange (Stratagene) kit and primers 5'-CTGGGCAGAGTGGTCCGGTCCGAAAGATG-3' and 5'-CATCTTTCGGACCGGACCACTCTGCCCAG-3'. The integrity of all constructs was verified by DNA sequencing.

BL21(DE3) cells harboring the above plasmids were grown to mid-exponential phase (A_{600} ≈ 0.5) in 500 mL of LB medium supplemented with 34 μg/mL chloramphenicol. Protein synthesis was initiated by addition of 0.4 mM isopropylthiogalactopyranoside (IPTG) and cultures were immediately transferred to a water bath held at 25°C. After 4h incubation at this temperature, cells were sedimented by centrifugation at 3,000 *g* for 15 min, resuspended in 20 mM Tris-HCl, pH 7.5, 2.5 mM EDTA, 1 mM PMSF to a concentration of 100 A_{600} units per mL, and disrupted by three cycles of homogenization on a French pressure cell operated at 10,000 psi. Insoluble material was removed by centrifugation at 14,000 *g* for 15 min. Aliquots of clarified extracts (≈15 mL) were transferred to 30 mL Corex tubes and held in an 80°C water bath for 10 min to precipitate the majority of host proteins. Aggregated fractions were removed by centrifugation at 14,000 *g* for 10 min. Supernatants were diluted with 60 mL of buffer A (20 mM Tris-HCl, pH 7.5) and loaded onto a DE52 (Whatman) anion exchange column (7.0 cm length by 1.0 cm in diameter) equilibrated in buffer A. The column was developed in the same buffer at 1 mL/min for 60 min to wash out contaminants and purified designer proteins were recovered in the 25–100 mM NaCl fractions of a 60 min gradient elution (0 to 500 mM NaCl in buffer A). Proteins were dialyzed against ddH_2O overnight and stored at −80°C. Purity was determined on overloaded gels using a modified SDS-PAGE protocol.[33]

Biomineralization of CaP Nanoparticles

For biomineralization experiments, a 1.8 mL solution containing 5 μM of protein in 1 mM $(NH_4)_2HPO_4/NH_4H_2PO_4$, pH 7.5 was placed in a 15 mL, round bottom, disposable borosilicate tube (VWR) that had been cleaned with ddH_2O, acetic acid, acetone, and ultrapure ddH_2O, in sequence and fitted with a 1 cm diameter stirring bar. The mixture was held at 4°C for 30 min at a stirring rate of 6 (Corning PC-310), after which 200 μL of a 16.7 mM solution of $Ca(NO_3)_2$ was fed in 8 μL increments about 5 seconds apart using a 25G delivery needle or Pipetman (Eppendorf P20). The mixture was allowed to age for 2h at 4°C and held at room temperature for 12–24h before characterization.

Analytical Techniques

Hydrodynamic diameters were measured by dynamic light scattering (DLS) on a Nano-ZS Zetasizer (Malvern). For TEM imaging, 5 μL of solution was deposited on a carbon-coated copper TEM grid and allowed to air dry. Low and high resolution TEM images, selected area electron diffraction (SAED) patterns with aperture size 40 μm were collected on a FEI

Tecnai G2 F20 S/TEM operated at an accelerating voltage of 200 kV. For SEM imaging, samples (≈ 100 μL) were allowed to contact a clean, ≈ 1 cm^2 silicon wafers for 30 min and excess fluid was removed by wicking with a laboratory tissue. The substrate was rinsed with ddH_2O to remove salts, air dried and coated with a 7–10 nm Au/Pd film. Micrographs were taken with a FEI Sirion SEM at 10 keV acceleration voltage. Energy dispersive x-ray spectroscopy (EDS) was used to find the average ratio of calcium, phosphorus, and oxygen in the substrate. X-ray diffraction (XRD) measurements were conducted on a Bruker D8 Focus using CuKα radiation. Data were collected for 2θ values ranging from 22 to 42° with 0.02° steps.

Animal Studies

The adjuvancy effect of biofabricated CaP nanoparticles was compared to that of AdjuPhos™ (Brenntag Biosector), a commercial aluminum phosphate adjuvant consisting of 0.49% (wt/wt) aluminum and 1.52% phosphate. CaP nanoparticles were synthesized using TrxA::PA44 as described in section 2.4 except that all solutions were made in endotoxin-free water (MD Bio) and that all glassware was passivated by rinsing in tap water, acetic acid, ddH_2O, acetone, and ultrapure ddH_2O before autoclaving at 120°C for 30 min and inactivating pyrogens by heating for 30 min in a 250°C oven. After 2h of aging at 4°C, samples were filtered through a 0.22 μm cellulose acetate filter and split in two halves, one of which was used for DLS characterization and protein assays and the other for immunization in mice. The final protein concentration was found to be 3.2 μM by Bradford assay due to losses incurred during filtration. However, the size of the particles remained in the 70 nm range. As a control, a preparation of 3.2 μM TrxA::PA44 in 1 mM $(NH_4)_2HPO_4$/$NH_4H_2PO_4$, pH 7.5 was filtered through a 0.22 μm membrane and supplemented with 1.65 mM of AdjuPhos (an aluminum concentration identical to that of the calcium in the nanoparticles). Groups of five C57BL/6 mice (6–10 weeks old and weighing 20–30 g) were injected subcutaneously with 4 × 50 μL of the above preparations into the four foot pads for a total antigen load of 8 μg. No inflammation was observed at injection sites and animals were bled at 9 and 21 days. Anti-TrxA IgG titers were measured in serum by ELISA essentially as described[34] using plates coated with wild type TrxA and validated for linearity with mouse anti-TrxA rabbit monoclonal antibodies (Invitrogen, clone C63C6).

RESULTS

Selection of Calcium Phosphate Binding Peptides

Among the various inorganic compounds that hold promise for DC maturation, we selected calcium phosphate (CaP) because it is cheap, biocompatible, biodegradable, and likely to be safe. CaP adjuvants are typically synthesized by uncontrolled precipitation schemes, yielding a broad distribution of agglomerates that range in size from 300 nm to 4 μm and have calcium to phosphate (Ca:P) molar ratios from 1.35 to 1.83.[35] In one of the most detailed analyses to date, Jiang and coworkers[36] reported that a commercial adjuvant manufactured by the former Reheis Inc. consisted of calcium-deficient hydroxyapatite with a Ca:P ratio of 1.39, and contained needle-like particles and irregularly-shaped plates. However, others[37] have found commercial adjuvants to have a Ca:P ratio of 1.5, a molecular composition closer to that of tricalcium phosphate ($Ca_3(PO_4)_2$).

Our first task was to generate CaP “chips” that were chemically and morphologically representative of commercial CaP adjuvants, and compatible with the FliTrx cell surface display system that we have previously used to identify SBPs.[28, 31] To this end, we electrodeposited ≈10 μm thick calcium phosphate films on titanium foil from a $Ca(NO_3)_2$/$NH_4H_2PO_4$ electrolyte (section 2.1). Because annealing at high temperatures drives off coordinated water from inorganic materials, half of the samples were annealed by heating at

450°C for 8h while the rest were dried under a nitrogen stream and characterized as deposited.

SEM imaging revealed that the annealed samples (Fig. 1C–D) consisted primarily of spherical nodules while non-annealed chips also contained crystalline platelets and needles (Fig. 1A–B). The Ca:P ratio was found to be 1.44 for annealed samples and 1.32 for non-annealed samples by Energy Dispersive X-ray spectroscopy (EDS) analysis in the SEM. In addition, reflections characteristic of calcium phosphate-containing phases were identified in the 26° and 31–34° 2θ regions of both samples by X-ray diffraction (XRD; Fig. 1E). Thus, our electrodeposited CaP chips are compositionally and morphologically similar to typical calcium phosphate adjuvants.[35–37]

In the *E. coli* FliTrx cell surface display system,[38] random dodecapeptides are displayed as disulfide-constrained loops within the active site of *E. coli* Thioredoxin 1 (TrxA) which is itself inserted within the major flagellar protein FliC. We used FliTrx biopanning to isolate CaP-binding peptides on both annealed and non-annealed substrates. Because there are multiple solutions to the problem of inorganic binding,[21] sequences obtained after biopanning did not converge towards a consensus. We arbitrarily chose a subset of 6 sequences exhibiting a broad range of pIs and hydrophilicities for further work with the expectation that some of them would function as efficient CaP mineralizers. Three of these CaP-binding peptides (PN series) were isolated using the non-annealed chip, while the others (PA series) were selected on the annealed substrate (Table 1).

Protein-Aided Mineralization of CaP Nanoparticles

An accurate comparison of the mineralizing ability of the above CaP binders would ideally require that they exhibit the same solubility (which is generally not true of short hydrophobic peptides such as those listed in Table 1) and that they are displayed within the same structural context. To address this issue, we constructed a series of *E. coli* TrxA derivatives in which the authentic cysteine-glycine-proline-cysteine (CGPC) active site sequence was replaced by one of the CaP-binding dodecamers in Table 1 flanked by invariant Cys-Gly-Pro (CGP) and Gly-Pro-Cys tripeptides (GPC). The resulting proteins, which are monomeric and range in molecular mass from 12.87 to 13.14-kDa, were expressed at about 35% of the total cellular protein and in a mostly soluble form using T7 driven transcription (Fig. 2, lanes 1–3). Because TrxA exhibits high thermostability,[39] it was possible to achieve 80% purification by heating crude cell extracts at 80°C for 10 min and removing aggregated host proteins by centrifugation (Fig. 2, lanes 4–5). High purity material (≈ 99%) could then be recovered in a single ion exchange chromatography step (Fig. 2, lane 6).

Because calcium phosphate does not exhibit useful optical absorption or emission properties, we screened CaP-binding TrxA derivatives for their ability to mediate nanoparticle formation using dynamic light scattering (DLS), a technique that provides information on the hydrodynamic diameter of colloids in suspension. We dedicated significant effort at optimizing the synthesis step, testing different calcium and phosphate salts, pH, protein concentrations, mixing regimes, temperatures and aging times, eventually settling on the protocol described in section 2.4. Experiments conducted in the absence of protein or with wild type TrxA gave rise to the precipitation of large polydisperse species (Fig. 3A–B). However, among the six proteins tested, three (TrxA::PN21, TrxA::PN38 and TrxA::PA44) proved suitable for the reproducible production of sub-100 nm CaP particles. Of note, TrxA::PA01 was ineffective in mediating nanoparticle formation in spite of the fact that the PA01 sequence was isolated multiple times on both annealed and non-annealed chips. Thus, there is no correlation between promiscuous binding and nanoparticle synthesis ability.

Hydrodynamic diameters determined by DLS were 70 ± 20 nm in the case of TrxA::PN21 and TrxA::PN38, and 60 ± 20 nm for TrxA::PA44. The colloids were clear and stable for at least 3 weeks of storage at 4°C, indicating the presence of a capping protein shell. TEM imaging of TrxA-PA44-mineralized samples (Fig. 3A–B) confirmed the presence of roughly spherical species that had an average diameter of 25 ± 5 nm (n = 110). The discrepancy with diameters obtained by DLS is likely due to the difficulty in obtaining good contrast when imaging CaP by TEM, and to the fact that hydrated particles are bounded by a protein shell that adds to their size. Based on the lack of observable particle faceting and the fact that selected area electron diffraction (SAED) patterns were diffused and lacked distinct rings or spots (Fig. 3C), it is likely that the templated material is amorphous calcium phosphate (ACP; $Ca_9(PO_4)_6$), a non-crystalline phase of calcium phosphate that is the initial solid precipitating from supersaturated solutions.[40]

Controlling Particle Size: Influence of the Disulfide Bond

CaP binding sequences are displayed within a disulfide-bonded loop both during the initial FliTrx screen and following transfer to the soluble TrxA scaffold. This conformational context has been shown to influence the adhesion of certain solid binding peptides to their cognate inorganics,[41–44] but how it impacts materialization remains unclear. In order to explore this issue, we use site-directed mutagenesis to convert the first cysteine residue of TrxA::PA44 to serine, and conducted side by side mineralization experiments with no protein, wild type TrxA, TrxA::PA44 and the TrxA::PA44C32S mutant. Samples were transferred to silicon oxide substrates, coated with a 7-to-10 nm layer of gold-palladium and imaged by SEM.

In agreement with DLS data and consistent with the low solubility product of calcium phosphate, precipitation in the absence of additive gave rise to heterogeneous populations enriched in micrometer size particles (Fig. 4A) while mineralization in the presence of wild type TrxA led to the formation of aggregates consisting of interconnected nodules extending over large dimensions (Fig. 4B). As expected from TEM imaging (Fig. 3), and in sharp contrast with the above, samples prepared in the presence of TrxA::PA44 were populated by discrete and mostly spherical particles whose mean size (70 ± 15 nm; n = 44) was within the expected range when taking into account the thickness of the Au/Pd coating. Remarkably, altering the conformation of the PA44 peptide by elimination of the disulfide bond led to a net reduction in the number of particles and a concomitant 3-fold increase in average diameter as determined by analysis of SEM images (170 ± 30 nm, n = 55) and confirmed by DLS measurements (210 ± 50 nm). Similar results were obtained when the same cysteine to serine substitution was introduced into TrxA::PN21. We conclude that the conformational context plays an important role in determining the affinity and/or capping ability of several of our binders, a feature that can be exploited for manufacturing core-shell particles of different sizes.

Immunogenicity

Conjugates between nanoparticles and antigenic molecules hold potential for effective vaccination owing to the fact that particles of diameter below 100 nm drain to the lymph nodes where the probability of encountering immature DCs increases.[6, 7] We therefore used TrxA::PA44 to synthesize CaP nanoparticles as above, except that depyrogenated glassware and endotoxin-free water were used in all steps and that the solution was filtered through a sterile 0.2 μm membrane to eliminate large particulate contaminants. Groups of five C57BL/6 mice were injected subcutaneously with the nanoparticle formulation (8 μg total protein load) or with the same amount of soluble TrxA::PA44 supplemented with enough of the commercial adjuvant AdjuPhos so that the Al^{3+} concentration would equal that of Ca^{2+} in the nanoparticulate formulation. After 9 days, anti-TrxA titers were slightly higher in the

serum of nanoparticle-treated animals relative to control mice (Fig. 5). However, whereas antibody levels remained constant over time in the control group, they were more than 3-times higher in mice vaccinated with the nanoparticle formulation 21-days post challenge.

DISCUSSION

We have isolated disulfide-constrained dodecapeptides suitable for the synthesis of stable sub-100 nm nanoparticles consisting of an ACP core stabilized by a protein shell. The three sequences supporting nanoparticle formation (PA44, PN21 and PN38; Table 1) contained at least two, and up to four negatively charged aspartates (D) and/or glutamates (E). Enrichment in these acidic amino acids was not unexpected since they have high affinity for Ca^{2+} ions and are found at high proportions and local densities among proteins involved in biological apatite formation.[18,19] In contrast, the three CaP binders that failed to yield stable nanoparticles (PN52, PA01 and PA93) all contained three or more basic residues and carried a net positive charge under our synthesis conditions (pH 7.5). Remarkably, hydroxyapatite-binders identified by others through bacteriophage display (Table 1) were also enriched in histidines (H), arginines (R), and lysines (K). Two of these peptides were tested for CaP mineralization, albeit under different conditions compared to the present study and to each other. In a synthetic form, peptide HABP1 caused the formation ofoctacalcium phosphate (OCP; $Ca_8H_2(PO_4)_6{\bullet}5H_2O$) crystals that projected from a central core and were 400 to 800 nm in width and several μm in length.[45] Synthetic CLP12 promoted the mineralization of μm-sized hydroxyapatite plates made up of randomly oriented ≈ 20 nm nanocrystals.[46] It is therefore clear that acidic amino acids are not absolutely required for a peptide to either bind CaP or to template the mineralization of thermodynamically stable calcium phosphate polymorphs (e.g., HA and OCP). However, our results suggest that aspartic and glutamic acid are important for capping and stabilizing nanoscale clusters of ACP, which should be the first CaP phase to precipitate out of solution.[40] Considering that ACP can convert to more energetically favorable phases such as OCP and biological apatites,[47] it is tempting to hypothesize that transient sequestration of ACP nanoparticles could be one of the mechanisms by which acidic bone and enamel-associated proteins regulate biomineralization. This process would be a useful complement to face-specific adsorption mechanisms[20] in preventing runaway crystal growth.

The phage and cell surface display libraries that are typically used to pan for solid binding peptides (SBPs) can yield linear or disulfide-bonded sequences.[21] In traditional applications (e.g., epitope mapping and identification of protein interaction domains), disulfide-bonded peptides are generally more efficient binders because they exhibit a low degree of conformational freedom and make stable contacts with protein targets. In solid binding, however, the impact of conformational flexibility is less clear. For instance, we previously reported that presentation in a disulfide-constrained loop is critical for a cuprous oxide binding peptide to adhere to this material.[42] Similarly, a disulfide-bonded conformation increased the affinity of both a platinum-and a gold-binding peptide for Pt and Au surfaces (respectively) relative to the corresponding linear conformations.[43, 44] By contrast, presentation in a loop had no effect on the adsorption behavior of a different gold binder[43] and decreased the affinity of a TiO_2/SiO_2 binding peptide for these oxides.[41] PA44 and PN21 likely belong to the former category of solid binders since a lower affinity of TrxA::PA44C32S (and TrxA::PN21C32S) for CaP, paired with the rapid kinetics of ACP formation,[47] would manifest itself by the growth of larger particles before protein capping occurs. From a practical standpoint, the ability to manipulate particle size via a single mutation in the CaP binding sequence should prove useful for tethering different loads of protein/antigen on the nanoparticle surface.

The observation that nanoparticles smaller than 100 nm in diameter preferentially accumulate in the lymph nodes where they encounter a high concentration of immature DCs has been exploited to design synthetic nanovaccines that are more efficient at triggering adaptive immunity.[6, 48–50] The TrxA::PA44-mineralized particles described herein are in the proper size range for effective diffusion into the lymphatic system and comprise a CaP core that may serve as a "danger signal" to activate DC maturation. As a preliminary test of our design, we vaccinated mice with TrxA::PA44 that was either in a nanoparticle-bound formulation or supplemented with the commercial adjuvant AdjuPhos. We found that although anti-TrxA levels were comparable in the two cohorts 9 days post-injection, there was three times more anti-TrxA in the serum of animals vaccinated with nanoparticles compared to the control group ($p < 0.05$) after 3 weeks. We are aware that absolute antibody titers were low, which is likely due to the fact that *E. coli* TrxA is 30% identical to mouse TrxA and a poor immunogen. Nevertheless, our results suggest that direct mineralization of antigen shell CaP core nanoparticles might be a simple and cost-effective route for nanovaccine manufacturing. We are currently exploring this concept further using TrxA::PA44-Ovalbumin fusion proteins.

CONCLUSIONS

We have identified CaP-binding dodecapeptides that are acidic and suitable for the synthesis of calcium phosphate core protein shell nanoparticles. The hydrodynamic diameter of these hybrid structures can be varied from about 60 nm to approximately 200 nm by eliminating the disulfide bond holding the CaP binding sequence in a constrained loop. Considering that the nanoparticle formulation enhances TrxA immunogenicity and because TrxA fusions are easy to construct and purify, such inorganic core protein shell architectures might prove useful for adjuvanted antigen delivery to DCs.

Abbreviations

ACP	amorphous carbon phosphate
CaP	calcium phosphate
TrxA	*E. coli* thioredoxin 1
ACP	amorphous calcium phosphate
DC	dendritic cell
HA	hydroxyapatite
SBP	solid binding peptides
OCP	octacalcium phosphate

Acknowledgments

We are grateful to Zahra Afsharinejad for performing the ELISA assays and to Shobana Vaidyanathan for help with animal studies. This work was supported by a Grand Challenge Exploration grant from the Bill and Melinda Gates Foundation, a NSF-NIRT award on Protein-Aided Nanomanufacturing (CMMI-0709131), the NSF Genetically Engineered Materials Science and Engineering Center (DMR-0520657) and NIH awards P30ES007033 and U19ES019545. Part of the work was conducted at the University of Washington Nanotech User Facility, a member of the NSF National Nanotechnology Infrastructure Network.

REFERENCES

1. Bose S, Tarafder S. Calcium phosphate ceramic systems in growth factor and drug delivery for bone tissue engineering: A review. Acta Biomater. 2011

2. Uskoković V, Uskoković DP. Nanosized hydroxyapatite and other calcium phosphates: chemistry of formation and application as drug and gene delivery agents. J Biomed Mater Res B Appl Biomater. 2011; 96:152–191. [PubMed: 21061364]
3. Aggerbeck H, Fenger C, Heron I. Booster vaccination against diphtheria and tetanus in man - comparison of calcium-phosphate and Aaluminum hydroxide as adjuvants. Vaccine. 1995; 13:1366–1374. [PubMed: 8585295]
4. He Q, Mitchell A, Morcol T, Bell SJD. Calcium phosphate nanoparticles induce mucosal immunity and protection against herpes simplex virus type 2. Clin Diagn Lab Immunol. 2002; 9:1021–1024. [PubMed: 12204953]
5. He Q, Mitchell AR, Johnson SL, Wagner-Bartak C, Morcol T, Bell SJD. Calcium phosphate nanoparticle adjuvant. Clin Diagn Lab Immunol. 2000; 7:899–903. [PubMed: 11063495]
6. Manalova V, Flace A, Bauer M, Schwarz K, Saudan P, Bachman MF. Nanoparticles target distinct dendritic cell populations according to their size. Eur J. Immunol. 2008; 38:1404–1413. [PubMed: 18389478]
7. Reddy ST, Rehor A, Schmoekel HG, Hubbell JA, Swartz MA. In vivo targeting of dendritic cells in lymph nodes with poly(propylene sulfide) nanoparticles. J. Control. Release. 2006; 112:26–34. [PubMed: 16529839]
8. Al-Qasas NS, Rohani S. Synthesis of pure hydroxyapatite and the effect of synthesis conditions on its yield, crystallinity, morphology and mean particle size. Sep Sci Technol. 2005; 40:3187–3224.
9. Ferraz MP, Monteiro FJ, Manuel CM. Hydroxyapatite nanoparticles: a review of preparation methodologies. J Appl Biomat Biomech. 2004; 2:74–80.
10. Rodriguez-Lorenzo LM, Vallet-Regi M. Controlled crystallization of calcium phosphate apatites. Chem Mater. 2000; 12:2460–2465.
11. Bose S, Saha SK. Synthesis and characterization of hydroxyapatite nanopowders by emulsion technique. Chem Mater. 2003; 15:4464–4469.
12. Morgan TT, Muddana HS, Altinoglu EI, Rouse SM, Tabaković A, Tabouillot T, Russin TJ, Shanmugavelandy SS, Butler PJ, Eklund PC, Yun JK, Kester M, Adair JH. Encapsulation of organic molecules in calcium phosphate nanocomposite particles for intracellular imaging and drug delivery. Nano Lett. 2008; 8:4108–4115. [PubMed: 19367837]
13. Roy I, Mitra S, Maitra A, Mozumdar S. Calcium phosphate nanoparticles as novel non-viral vectors for targeted gene delivery. Int J Pharm. 2003; 250:25–33. [PubMed: 12480270]
14. Martins MA, Santos C, Almeida MM, Costa ME. Hydroxyapatite micro- and nanoparticles: nucleation and growth mechanisms in the presence of citrate species. J Colloid Interface Sci. 2008; 318:210–216. [PubMed: 17996882]
15. Cai YR, Liu YK, Yan WQ, Hu QH, Tao JH, Zhang M, Shi ZL, Tang RK. Role of hydroxyapatite nanoparticle size in bone cell proliferation. J Mater Chem. 2007; 17:3780–3787.
16. Ganesan K, Kovtun A, Neumann S, Heumann R, Epple M. Calcium phosphate nanoparticles: colloidally stabilized and made fluorescent by a phosphate-functionalized porphyrin. J Mater Chem. 2008; 18:3655–3661.
17. Welzel T, Meyer-Zaika W, Epple M. Continuous preparation of functionalised calcium phosphate nanoparticles with adjustable crystallinity. Chem Commun. 2004; 21:1204–1205.
18. Palmer LC, Newcomb CJ, Kaltz SR, Spoerke ED, Stupp SI. Biomimetic systems for hydroxyapatite mineralization inspired by bone and enamel. Chem Rev. 2008; 108:4754–4783. [PubMed: 19006400]
19. George A, Veis A. Phosphorylated proteins and control over apatite nucleation, crystal growth and inhibition. Chem Rev. 2008; 108:4670–4693. [PubMed: 18831570]
20. Hunter GK, O'Young J, Grohe B, Karttunen M, Golberg HA. The flexible polyelectrolyte hypothesis of protein-biomineral interaction. Langmuir. 2010; 26:18639–18646. [PubMed: 20527831]
21. Baneyx F, Schwartz DT. Selection and analysis of solid-binding peptides. Curr. Opin. Biotechnol. 2007; 18:312–317. [PubMed: 17616387]
22. Dickerson MB, Sandhage KH, Naik RR. Protein- and peptide directed synthesis of inorganic materials. Chem Rev. 2008; 108:4935–4978. [PubMed: 18973389]

23. Sarikaya M, Tamerler C, Jen AK, Schulten K, Baneyx F. Molecular biomimetics: nanotechnology through biology. Nat Mater. 2003; 2:577–585. [PubMed: 12951599]
24. Sarikaya M, Tamerler C, Schwartz DT, Baneyx F. Materials assembly and formation using engineered polypeptides. Annu Rev Mater Res. 2004; 34:373–408.
25. Dai H, Choe WS, Thai CK, Sarikaya M, Traxler BA, Baneyx F, Schwartz DT. Nonequilibrium synthesis and assembly of hybrid inorganic-protein nanostructures using an engineered DNA binding protein. J Am Chem Soc. 2005; 127:15637–15643. [PubMed: 16262431]
26. Grosh C, Schwartz DT, Baneyx F. Protein-based control of silver growth habit using electrochemical deposition. Cryst Growth Des. 2009; 9:4401–4406.
27. Zhou W, Baneyx F. Aqueous, protein-driven synthesis of transition metal-doped ZnS immuno-quantum dots. ACS Nano. 2011; 5:8013–8018. [PubMed: 21942544]
28. Zhou W, Schwartz DT, Baneyx F. Single pot biofabrication of zinc sulfide immuno-quantum dots. J. Am. Chem. Soc. 2010; 132:4731–4738. [PubMed: 20218715]
29. Balamurugan A, Benhayoune H, Dumelie N, Laquerriere P, Ferreira JMF. Electrodeposition of fluorine-doped calcium phosphate coatings onto Ti6Al4V alloy - chemical and structural characterization. J. Am. Ceram. Soc. 2008; 91:2797–2801.
30. Dumelie N, Benhayoune H, Richard D, Laurent-Maquin D, Balossier G. In vitro precipitation of electrodeposited calcium-deficient hydroxyapatite coatings on Ti6Al4V substrate. Materials Char. 2008; 59:129–133.
31. Thai CK, Dai H, Sastry MS, Sarikaya M, Schwartz DT, Baneyx F. Identification and characterization of Cu2O- and ZnO-binding polypeptides by *Escherichia coli* cell surface display: toward an understanding of metal oxide binding. Biotechnol Bioeng. 2004; 87:129–137. [PubMed: 15236241]
32. Yasukawa T, Kanei-Ishii C, Maekawa T, Fujimoto J, Yamamoto T, Ishii S. Increase of solubility of foreign proteins in *Escherichia coli*by coproduction of the bacterial thioredoxin. J. Biol. Chem. 1995; 270:25328–25331. [PubMed: 7592692]
33. Okajima T, Tanabe T, Yasuda T. Nonurea sodium dodecyl sulfate-polyacrylamide gel electrophoresis with high-molarity buffers for the separation of proteins and peptides. Anal Biochem. 1993; 211:293–300. [PubMed: 8317706]
34. Zhang W, Zhang W, Tang Y, Zhang J, Liu JN. Characterization of an anti-thioredoxin monoclonal antibody. Biotechnol Lett. 2006; 28:183–188. [PubMed: 16489496]
35. Gupta, RK.; Rost, BE.; Relyved, E.; Siber, GR. Vaccine design. In: Powell, MF.; Newman, MJ., editors. Vaccine design. New York: Plenum Press; 1995. p. 239-241.
36. Jiang D, Premachandra GS, Johnston C, Hem SL. Structure and adsorption properties of commercial calcium phosphate adjuvant. Vaccine. 2004; 23:693–698. [PubMed: 15542192]
37. Relyved EH. Preparation and use of calcium phosphate adsorbed vaccines. Dev. Biol. Stand. 1986; 65:131–136. [PubMed: 3549396]
38. Lu Z, Murray KS, Van Cleave V, LaVallie ER, Stahl ML, McCoy JM. Expression of thioredoxin random peptide libraries on the *Escherichia coli* cell surface as functional fusions to flagellin: a system designed for exploring protein-protein interactions. Biotechnology. 1995; 13:366–372. [PubMed: 9634778]
39. LaVallie ER, DiBlasio EA, Kovacic S, Grant KL, Schendel PF, McCoy JM. A thioredoxin gene fusion expression system that circumvents inclusion body formation in the *E coli* cytoplasm. Biotechnology (NY). 1993; 11:187–193.
40. Zhao J, Liu YJ, Sun W-B, Zhang H. Amorphous calcium phosphate and its applications in dentistry. Chem Central J. 2011; 5:40.
41. Chen HB, Su XD, Neoh K-G, Choe WS. Context-dependent adsorption behavior of cyclic and linear peptides on metal oxide. Langmuir. 2009; 25:1588–1593. [PubMed: 19170646]
42. Choe WS, Sastry MSR, Thai CK, Dai H, Schwartz DT, Baneyx F. Conformational control of inorganic adhesion in a designer protein engineered for cuprous oxide binding. Langmuir. 2007; 23:11347–11350. [PubMed: 17918983]
43. Hnilova M, Oren EE, Seker UOS, Wilson BR, Collino S, Evans JS, Tamerler C, Sarikaya M. Effect of molecular conformations on the adsorption behavior of gold-binding peptides. Langmuir. 2008; 24:12440–12445. [PubMed: 18839975]

44. Seker UOS, Wilson B, Dincer S, Kim IW, Oren EE, Evans JS, Tamerler C, Sarikaya M. Adsorption behavior of linear and cyclic genetically engineered platinum binding peptides. Langmuir. 2007; 23:7895–7900. [PubMed: 17579466]
45. Gungormus M, Fong H, Kim IL, Evans JS, Tamerler C, Sarikaya M. Regulation of in vitro calcium phosphate mineralization by combinatorially selected hydroxyapatite-binding peptides. Biomacromolecules. 2008; 9:966–973. [PubMed: 18271563]
46. Chung WJ, Kwon KY, Song J, Lee SW. Evolutionary screening of collagen-like peptides that nucleate hydroxyapatite crystals. Langmuir. 2011; 27:7620–7628. [PubMed: 21291244]
47. Rabadjeva D, Gergulova R, Titorenkova R, Tepavitcharova S, Dyulgerova E, Balarew C, Petrov O. Biomimetic transformations of amorphous calcium phosphate: kinetic and thermodynamic studies. J Mater Sci Mater Med. 2010; 21:2501–2509. [PubMed: 20532962]
48. Fifis T, Gamvrellis A, Crimeen-Irwin B, Pietersz GA, Li J, Mottram PL, McKenzie IFC, Plebanski M. Size-dependent immunogenicity: therapeutic and protective properties of nano-vaccines against tumors. J Immunol. 2004; 173:3148–3154. [PubMed: 15322175]
49. Reddy ST, Swartz MA, Hubbell JA. Targeting dendritic cells with biomaterials: developing the next generation of vaccines. Trends Immunol. 2006; 27:573–579. [PubMed: 17049307]
50. Reddy ST, van der Vlies AJ, Simeoni E, Angeli V, Randolph GJ, O'Neil CP, Lee KL, Swartz MA, Hubbell JA. Exploiting lymphatic transport and complement activation in nanoparticle vaccines. Nat Biotechnol. 2007; 25:1159–1164. [PubMed: 17873867]
51. Weiger MC, Park JJ, Roy MD, Stafford CM, Karim A, Becker ML. Quantification of the binding affinity of a specific hydroxyapatite binding peptide. Biomaterials. 2010; 31:2955–2963. [PubMed: 20106520]
52. Segvich SJ, Smith HC, Kohn DH. The adsorption of preferential binding peptides to apatite-based materials. Biomaterials. 2009; 30:1287–1298. [PubMed: 19095299]

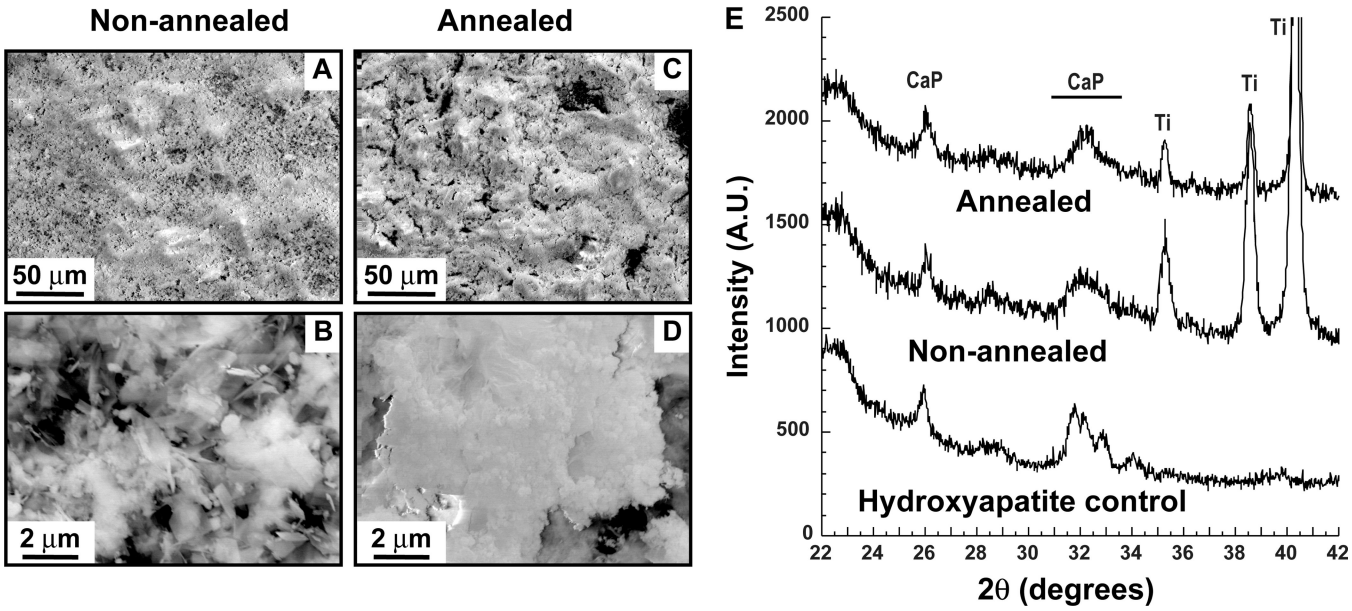

Figure 1.

Characterization of CaP chips. Non-annelaed (A–B) and annealed samples (C–D) were imaged by SEM at two different magnifications. Panel E shows XRD spectra for both samples. Hydroxyapatite powder was used as a control. Reflections corresponding to CaP phases and the underlying Ti substrate are labeled.

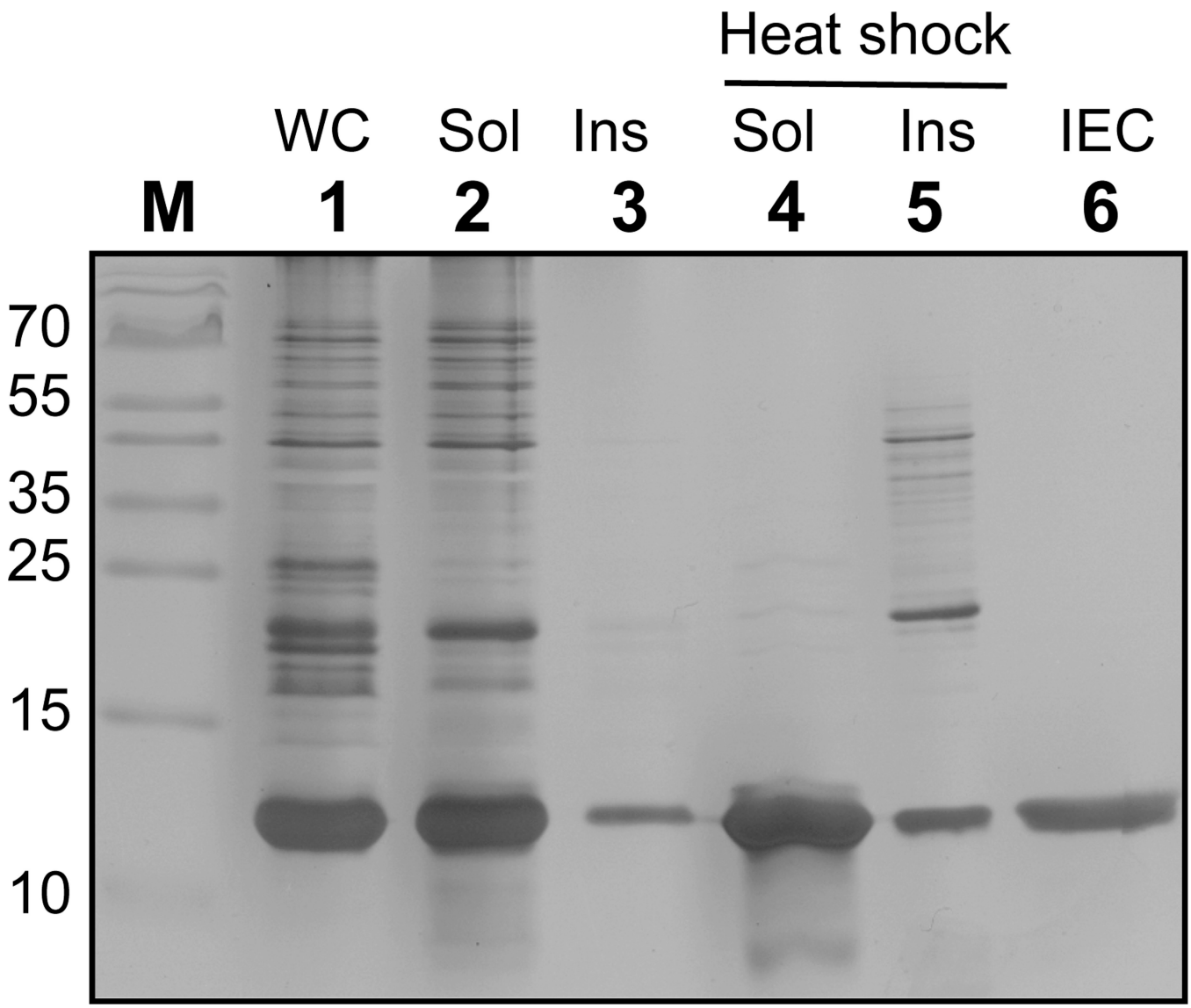

Figure 2.

Purification of TrxA::PA44 by heat shock and ion exchange chromatography (IEC). Lanes: M, markers; WC, whole cells; Sol and Ins: soluble and insoluble fractions before and after 10 min incubation at 80°C; IEC, ion exchange chromatography purification of heat-shocked soluble fractions. The position of the molecular mass markers (lane M) are indicated in kDa on the left of the gel which was silver-stained to reveal purified protein and contaminants.

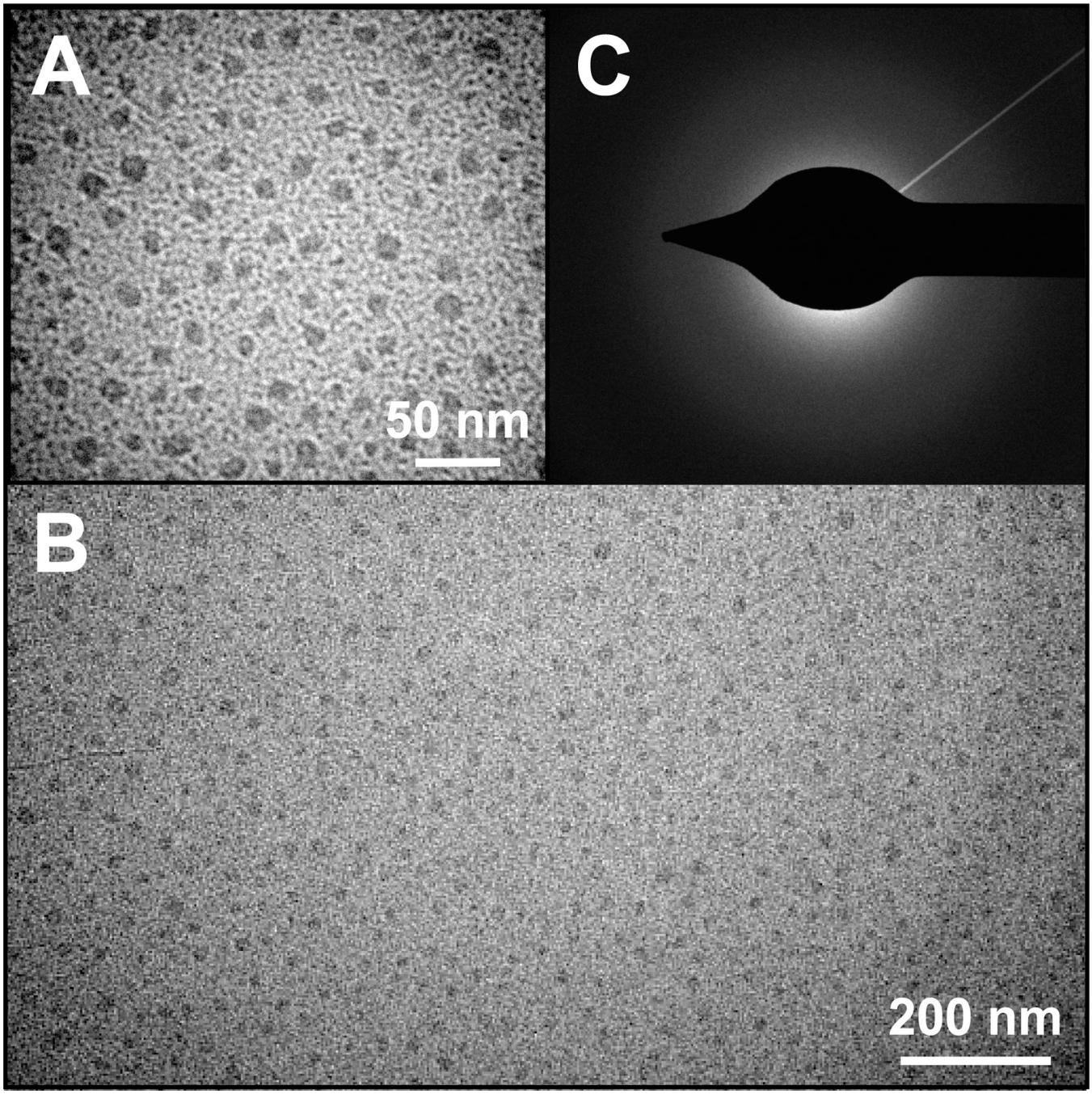

Figure 3.
TEM analysis of nanoparticles produced in the presence of TrxA::PA44. High (A) and low resolution (B) TEM images show that the characteristic size and polydispersity of CaP nanoparticles obtained under our experimental conditions. Selected area electron diffraction (SAED) patterns (C) were diffuse with no distinguishable spots or rings, suggesting that the mineral is amorphous calcium phosphate (ACP).

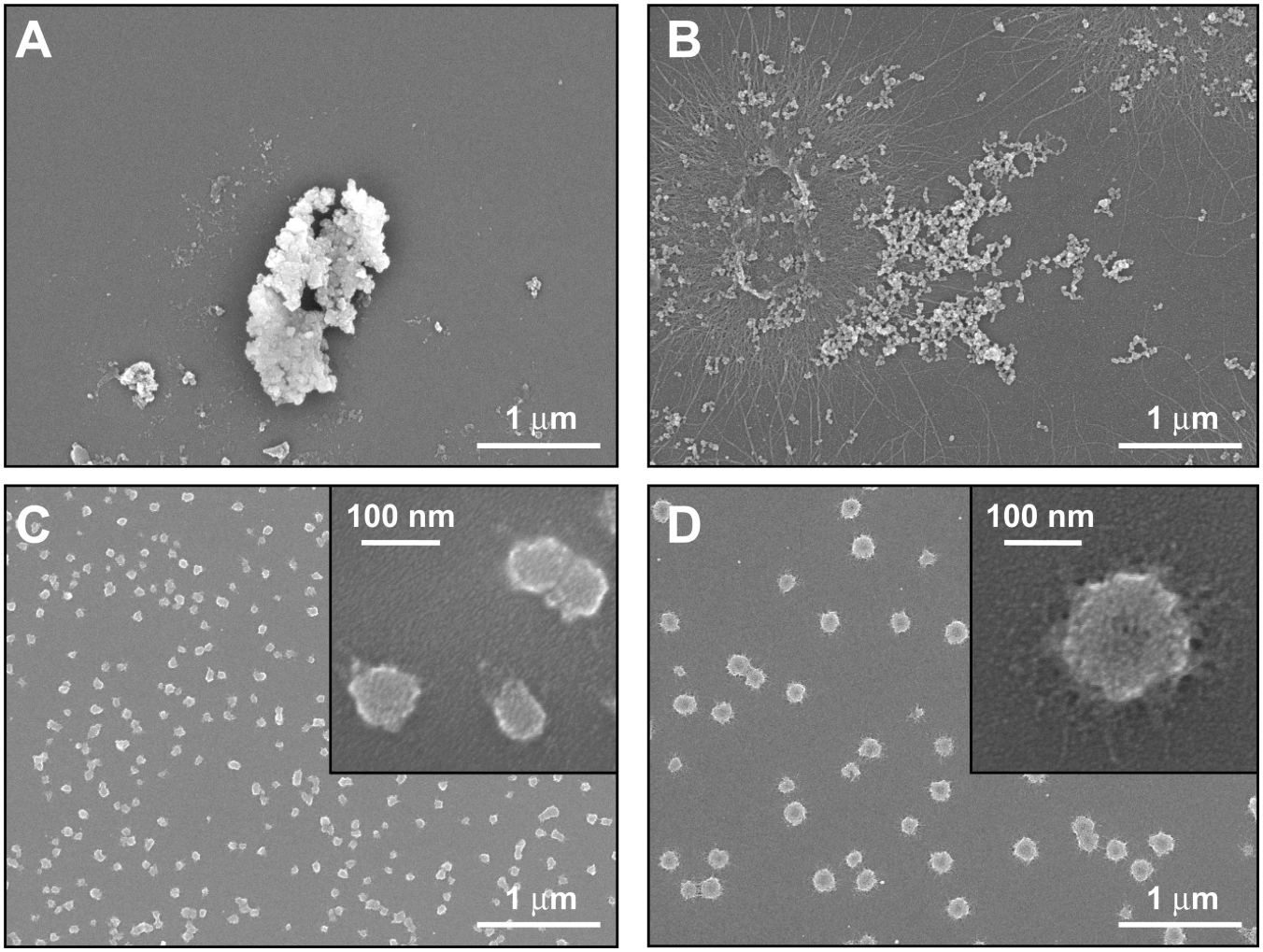

Figure 4.
SEM imaging of CaP structures mineralized in the absence of protein (A), or in the presence of wild type TrxA (B), TrxA::PA44 (C), and TrxA::PA44C32S. The inset of panels C and D show higher resolution images.

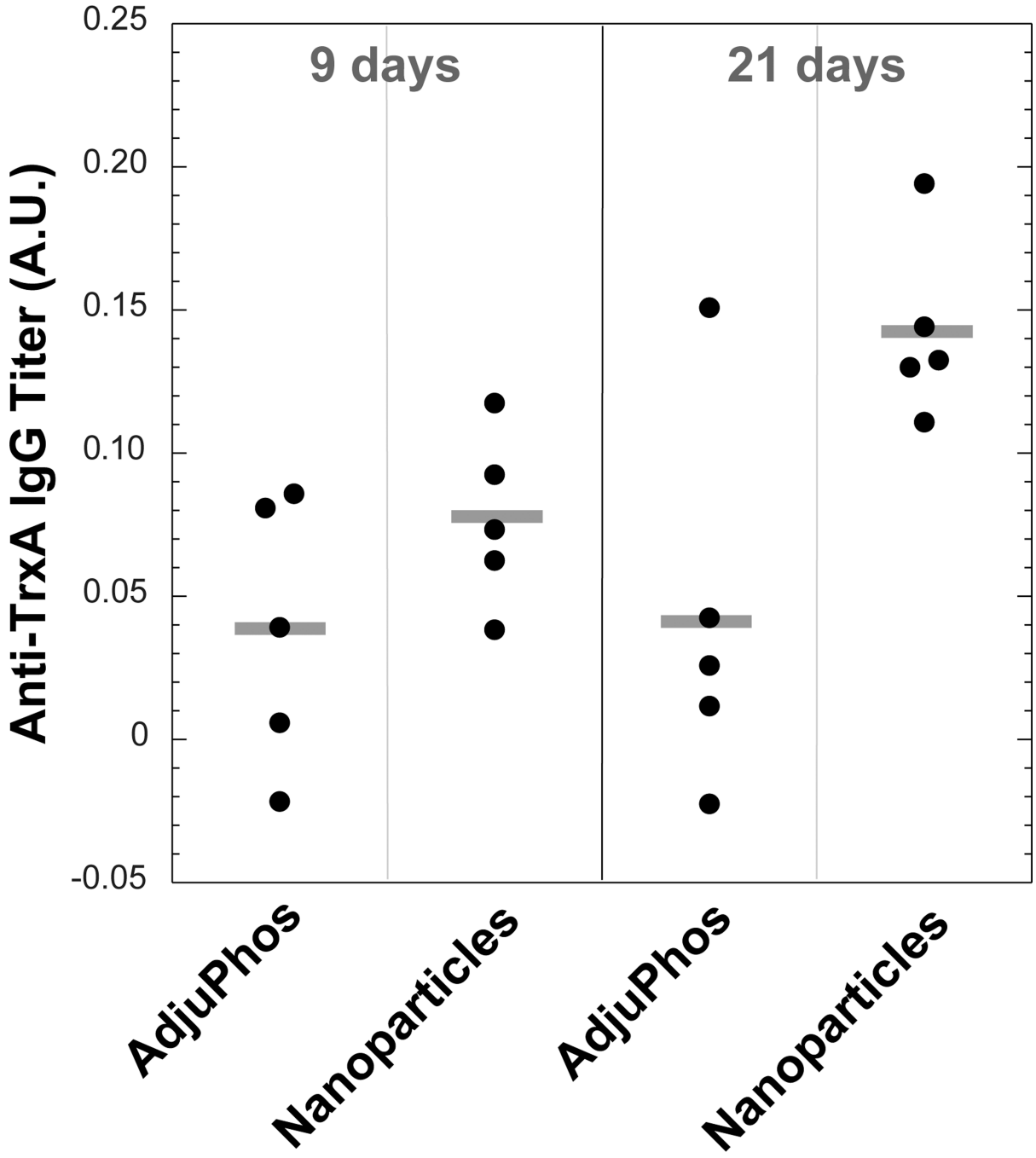

Figure 5.

Anti-TrxA IgG titers in the serum of C57BL/6 mice was measured by ELISA assay 9 and 21 days post-challenge with TrxA::PA44 and alum or TrxA::PA44-stabilized nanoparticles. Titers for individual animal and cohort means (horizontal bars) are shown. Data are corrected for pre-immune backgrounds. Confidence levels are 84.6% for 9 days data and 98.5% for 21 days data.

Table 1

Physico-chemical characteristics of CaP-binding peptides isolated by cell surface display and tested for mineralization ability (top) and comparison to hydroxyapatite binding peptides identified by phage display (bottom).

Name	Sequence[a]	M_r (Da)	pI	Hydropathy[b]	Reference
PN21	*CGP*LGMRSESAIGKE*GPC*	1277.4	6.14	−0.483	This work
PN38	*CGP*EDIDAVSVGEVQ*GPC*	1260.3	3.43	0.017	This work
PN52	*CGP*PAQAHPWPHRYG*GPC*	1416.5	9.18	−1.517	This work
PA01[c]	*CGP*VRRLMGGSWKRV*GPC*	1444.7	12.3	−0.483	This work
PA44	*CGP*KDVVVGVPGGQD*GPC*	1169.3	4.21	−0.033	This work
PA93	*CGP*GHLSPRFRGGRG*GPC*	1296.4	12.3	−1.175	This work
HABP1	*C*MLPHHGA*C*	761.9	6.69	−0.129	45
CLP12	NPYHPTIPQSVH	1389.5	6.92	−1.025	46
HA-1	SVSVGMKPSPRP	1214.4	11.0	−0.475	51
S	STLPIPHEFSRE	1412.5	5.38	−0.758	52
V	VTKHLNQISQSY	1417.5	8.57	−0.725	52

[a] Amino acids are color-coded as follows: hydrophobic, gray; acidic, red; basic, cyan; hydroxyl side chain, dark green; amide side chain, light green. Invariant tripeptides flanking the dodecamers are italicized.

[b] Positive hydropathy scores denote hydrophobic sequences while negative scores denote hydrophilic ones. The higher (respectively, lower) the score, the more hydrophobic (respectively, hydrophilic) the sequence is.

[c] The PA01 sequence was isolated over 50 times on both annealed and non-annealed samples.